ELSEVIER

Contents lists available at ScienceDirect

Powder Technology

journal homepage: www.journals.elsevier.com/powder-technology



Salt effect and comparative analysis of micro and nano-bentonite in blue dye removal: Surface morphology and adsorption efficiency

Hassan Wathiq Ayoob ^{a,b}, Nabil Kadhim Taieh ^{c,*}, Abdulrazzaq S. Abdullah ^d, Raad Z. Homod ^{e,*}, F. Medina ^b

- ^a Department of Chemical Engineering, College of Engineering, University of Basrah, Basrah, Iraq
- ^b Chemical Engineering Department, Rovira i Virgili University, Tarragona, Spain
- Dept. of Materials Engineering Technology, Technical Engineering College-Baghdad, Middle Technical University, Baghdad, Iraq
- d Chemical & Petrochemical Techniques Engineering Department, Basra Engineering Technical College, Southern Technical University, Basra, Iraq
- ^e Department of Oil and Gas Engineering, Basrah University for Oil and Gas, Basra, Iraq

HIGHLIGHTS

- The proposed technique improves adsorption capabilities for bentonite by applying nanotechnology (physical treatment).
- Research was done on the effects of salt at varying concentrations on the adsorption capacity.
- Micro/nano bentonites were characterized using AFM, BET, BJH, T-plots, and FTIR in two water types.
- The adsorption process was effectively fitted the models of Freundlich isotherm equilibrium and pseudo-second-order kinetic.

ARTICLE INFO A

Keywords:
Bentonite adsorption
Methylene blue removal
Nano-bentonite efficiency
Adsorption isotherms
Kinetic models and thermodynamics

GRAPHICAL ABSTRACT



ABSTRACT

Addressing contaminated water from various industrial practices has become a pressing concern. Methylene Blue (MB) dye is a prevalent industrial pollutant used in printing, dyeing, textiles, paper, plastics, and leather production. This study employed an efficient, cost-effective, environmentally friendly, and abundant adsorbent to remove Methylene Blue. Bentonite has been utilized as an adsorbent under varying dosages, acidity (pH), agitation, and salinity of contaminated wastewater. The adsorption capacity is enhanced by increasing the surface area and pore volume of the bentonite particles when they are transformed into nanoparticles. The adsorption capability increased with higher doses (10–50 mg) and longer shaking times (10–40 min), as well as with the concentration of the contaminated dye (5–25 ppm), but it decreased with rising pH values (2–12). The impact of temperature on the adsorption process was examined within the range of 25–55 °C. The results indicated that the adsorption capability is largely unaffected by wastewater salinity up to 10,000 ppm. The maximum adsorption capacities achieved under optimal conditions were 24.25 mg/g for micro-bentonite (μ B) and 40.75 mg/g for nano-bentonite (μ B), respectively. FTIR was employed to examine the adsorption of

E-mail addresses: hassan.wathiq@uobasrah.edu.iq (H.W. Ayoob), nabeel_khadum@mtu.edu.iq (N.K. Taieh), abdalmaliky@stu.edu.iq (A.S. Abdullah), raadahmood@yahoo.com (R.Z. Homod), francesc.medina@urv.cat (F. Medina).

^{*} Corresponding authors.

methylene blue dye by bentonite. BET, BJH, T-plots, and AFM analyses were conducted to determine the surface area, pore volume, pore diameter, and mean particle diameters for micro and nano bentonite. The results correlated more accurately using the Freundlich isotherm compared to the Langmuir and Tempkin models, due to its superior regression value (R^2) . The most suitable kinetic model for this investigation was the pseudo-second-order, in contrast to the pseudo-first-order, Elovich, and intra-particle diffusion models.

1. Introduction

Since pollution is one of the most significant and pervasive issues facing the world due to the accelerated expansion of industrial activities, protecting the environment—our habitat—must be our top priority. We regard water contamination as one of the most significant environmental challenges, given its critical importance in our daily lives. Water sources have seen significant degradation due to the daily discharge of hundreds of chemical compounds, either directly or indirectly [1]. Foreign substances or contaminants contaminate water, compromising its purity and posing a risk to individuals or the environment. Pigments are typically organic, either natural or synthetic chemicals utilized throughout several sectors, including painting and textile dyeing [2]. Synthetic dyes, extensively utilized as colorants in paper, wool, silk, cotton, food, cosmetics, and pharmaceutical industries, exhibit significant biodegradability challenges in the physical environment [3]. We can categorize dyes as anionic, cationic, and non-ionic. Several industries extensively utilize Methylene Blue, a cationic dye [4], leading to its significant consumption for industrial purposes. Each year, approximately 7 × 10⁷ tons of synthetic dyes are manufactured globally, with more than 10,000 tons utilized by the textile industry [5]. Methylene Blue is a functional dye that serves as a Red-X indicator and exhibits distinct colors (blue/colorless) in its oxidized and reduced forms. Tissue staining uses Methylene blue (Rahimian and Zarinabadi 2020) [6]. Synthetic dyes typically remain in the environment as they are not effectively removed by standard water treatment methods, owing to their great stability against temperature, light, water, and many compounds, including soaps and detergents [6]. Methylene Blue Dye (MB) can cause numerous health issues in humans, including cyanosis, tissue necrosis, Heinz body formation, vomiting, jaundice, shock, and increased heart rate [7]. The presence of MB poses significant challenges to plants, including growth suppression and decreased pigment and protein content in the microalgae Chlorella vulgaris and Spirulina platensis [8]. Consequently, the adverse impacts linked to wastewater containing MB dye necessitate efficient treatment before industrial discharge to mitigate the scarcity of clean water in society [9];. This phenomenon is prevalent in developing nations where substantial quantities of wastewater are discharged into the environment without adequate management [10]. Therefore, researchers have extensively employed a variety of treatment strategies, including biological methods (using enzymes and microorganisms), chemical methods (applying advanced oxidation processes), and physicochemical methods (primarily adsorption), to remove dye from the environment [11]. Methylene Blue Dye is an aromatic heterocyclic molecule with a flat shape [12] and It has a specific molecular weight and chemical structure [13]. MB dye is a common blue, cationic thiazine dye that is extensively used in the textile industry as a fiber coloring agent and in the medical profession as a staining agent for preventative and therapeutic purposes [14].

The challenge of water pollution is tackled using an innovative adsorption method with bentonite clay, chosen for its natural abundance, cost-effectiveness, and proven adsorption abilities, although its performance can vary depending on its geographical origin [15]. To improve treatment efficiency, the particle size is reduced to the nanoscale through physical grinding, which greatly increases the available surface area. This research advances beyond previous studies through three key contributions: first, a systematic comparison between microand nano-bentonite performance; second, an evaluation of adsorption efficiency under saline conditions (up to 10,000 ppm), addressing a

significant gap for industrial applications; and third, the use of advanced characterization techniques (BET, BJH, AFM) to establish detailed structure-function relationships. Unlike conventional studies that focus solely on adsorption capacity after reusability, a comprehensive assessment is made of pore architecture, particle size distribution, and regeneration potential. The stability of the adsorbent is demonstrated through multiple reuse cycles, with nano-bentonite maintaining 87 % efficiency after five uses. These results are supported by kinetic modelling, which identifies the pseudo-second-order mechanism as dominant. The integrated approach offers both fundamental insights into nanoscale adsorption phenomena and practical solutions for textile wastewater treatment, especially in saline environments. The environmental sustainability and economic feasibility of this modified bentonite system are emphasized, providing a scalable alternative to traditional treatment methods, with the reusability of bentonites for Methylene Blue Dye shown in Table 1.

2. Materials and methods

This section logically arranges the preparations by grouping related ideas together and, where possible, writing chronologically. We will briefly describe the subsections associated with the study as follows:

2.1. Materials

The unprocessed bentonite was acquired from Iraqi National Company for Geological Survey and Mining, Baghdad, Iraq. The chemical substances, comprising methylene blue trihydrate (MB) dye (C16H18ClN3S·3H2O, HIMEDIA, India), hydrochloric acid (HCl, 37 %, Spain), and sodium hydroxide (NaOH, United Kingdom), were acquired from Areej Al-Furat Co., Ltd. in Iraq.

2.2. Preparation of micro-bentonite and nano-bentonite

We pulverized the raw bentonite using a jaw crusher (Retsch, LABSCO, D-6360 Friedberg/H-Germany), subjected it to multiple washes with distilled water to eliminate contaminants, and subsequently dried it at 65 $^{\circ}$ C in a domestic oven (Silver Top, Germany). The bentonite utilized as an adsorbent was dried, crushed, and subjected to sieve analysis using a Retsch system (LABSCO, D-6360 Friedberg/H-Germany) with a no. 200 (75 μm) screen. Subsequently, a ball mill (LABSCO, D-6360 Friedberg/H-Germany) pulverized the bentonite particles to a nanoscale.

2.3. Preparation of dye solution

A mother solution of methylene blue dye (100 ppm) was generated by dissolving 0.1 g of dye (weighed using a calibrated four-digit balance, model: DENVER, Germany) in one liter of distilled water. We used a hot plate magnetic stirrer (LMS-1003D, Daihan Lab.Tech, Korea) operating at 1000 rpm and an ultrasonic bath (Model 031S) at 35 °C for 10 min to ensure complete dissolution of dye particles in water. We created dye concentrations ranging from 1 to 25 ppm using the dilution law. We generated a standard curve based on maximal dye adsorption at a wavelength of 665 nm, as is illustrated in Fig. 1. We used the UV–Vis spectrophotometer (pg, T80+, United Kingdom) to determine the residual dye concentration.

2.4. Batch adsorption for removal of methylene blue (M. B)

Batch studies were executed to examine the adsorption properties of M.B onto μB and nB, conducted at 25 °C on a rotary shaker water bath (HY-4 RECIPROCATED SHAKER) at 120 rpm. Different operating conditions were applied to get on the optimal adsorption conditions. Adsorbent dosage was experimented in the range of 10-80 mg.We used a Mi150 pH Meter (Martini, Romania) to set the value of the pH solution, which was varying from 2 to 10. We conducted adsorption kinetics over a time range of 10 to 60 min. We examined adsorption isotherms at varying starting dye concentrations (5–25 mg/L). All adsorption tests were performed in triplicate, and the average results were reported [23]. The values of relative standard deviation for adsorption isotherms and kinetics were under 4 %. The quantity of dye adsorbed and the clearance efficiency can be calculated using the formulae provided by [24]; [13].

$$qe = \frac{(Co - Ce) \times V}{m} \tag{1}$$

$$R(\%) = \frac{Co - Ce}{Co} \times 100 \tag{2}$$

In this context, q_e (mg/g) denotes to the quantity of adsorbed dye onto micro-bentonite and nano-bentonite; Co and Ce (mg/mL) represent the initial and equilibrium concentrations of dye, respectively; V (mL) indicates the volume of the solution; m (g) signifies the mass of the adsorbent; and R (%) refers to the percentage of dye removal.

3. Results and discussion

To easily follow the discussion, this section is divided into four subsections:

3.1. Materials' structure and properties

3.1.1. Surface morphology and particle size distribution

Atomic Force Microscopy (Nanosurf FlexAFM, Switzerland) was used to measure the particle size of Bentonite to look at the shape and distribution of micro- and nano-sized particles on the surface [25]. The AFM patterns for μ B (Fig. 2 a and b) and nB (Fig. 2 c and d) show that their surface morphology is very different, which could change how well they remove blue dye from water. Also, the height scales, which go from

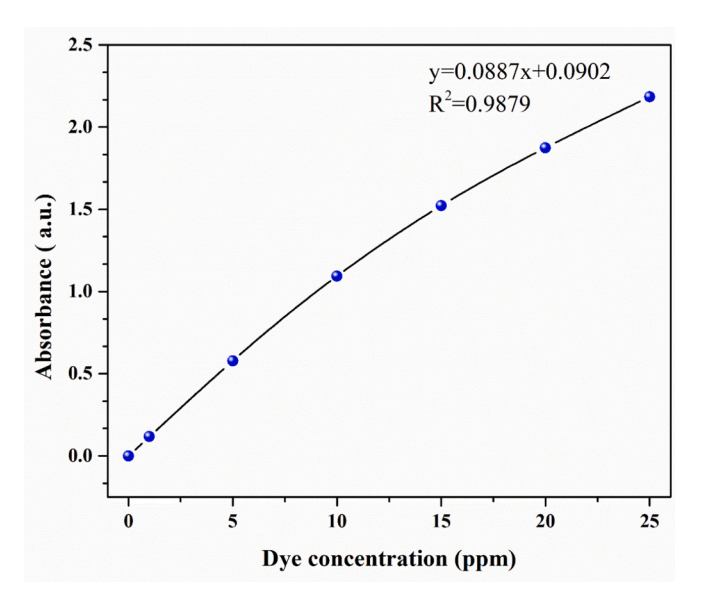


Fig. 1. Represent the absorbance empirical correlation of standard concentration.

696.6 nm in the 2D analysis (Figure a) to 607.7 nm in the 3D representation (Fig. 2b), show that the surface of µB is very different, indicating that it is highly textured and made up of large groups of particles. The AFM test result demonstrated that the mean diameter of μB is 140.3 nm, and its size distribution ranges from approximately 6.8 nm to 989.7 nm, as shown in Fig. 2b. Interestingly, the surface of the nB is significantly more even, and more uniform, with an appreciably smaller particle size; the max height in 2D analysis c is 24.66 nm, and it sticks to 12.67 nm in the 3D view. Nano-bentonite powder gave rise to innumerable other particles with an ever-decreasing mean size fraction of 10-30 nm, as shown in Fig. 2c. Most particles are also smaller than 40 nm, with an average of 30.04 nm. The results clearly show that the finer and well-dispersed nB particles could potentially influence the surface reactivity and functional properties that set it apart from µB. Nano-Bentonite has smaller particles, a more even distribution, and a higher surface area-to-volume ratio because of these surface features. These all help to improve adsorption and speed up the removal of blue dye

Represent bentonite was used (without chemical treatment) as an adsorbent in previous research to remove Methylene Blue Dye.

Adsorbate	Adsorption capacity (mg/g)	Mean Particle Diameter (nm)	Total Pore Volume (cm ³ /g)	Mean Pore Diameter (nm)	Surface Area (m²/g)	Adsorption capacity(mg/g) after 5 Cycles (Reusability)	Ref.
Pure bentonite (England)	-	40,000 (40 μm)	-	-	400	-	[16]
Yemen bentonite	417.4–500	-	0.109	-	82.3 (cm ² . g- ¹)	-	[15]
bentonite -Nador (Morocco)	62.5	-	-	-	-	-	[17]
Iraqi bentonite	21.79 (mg/L)	_	_	_	_	_	[18]
natural Iraqi bentonite	256	_	-	14.2	30.6	-	[19]
Libyan Bentonite - activated bentonite	4.3	-	-	-	-	-	[20]
Pure Bentonite (Semenyih, Malaysia)	21.131	-	0.22	-	8.86	-	[21]
Bentonite - Purified Bentonite Moroccan clay	681.85–1383	-	-	-	66.93–92.98 (m ² /g)	-	[22]
Iraqi micro-bentonite	24.05	140.3	BET 0.1023 BJH 0.097577 Lang. ——— t-Plot 0	11.111 - - -	36.832 30.102 43.007 38.554	20.44	This work
Iraqi nano-bentonite	40.33	30.04	BET 0.1302 BJH 0.1235 Lang. —— t-Plot 0	10.995 - - -	47.37 36.474 57.47 49.421	35.08	This work

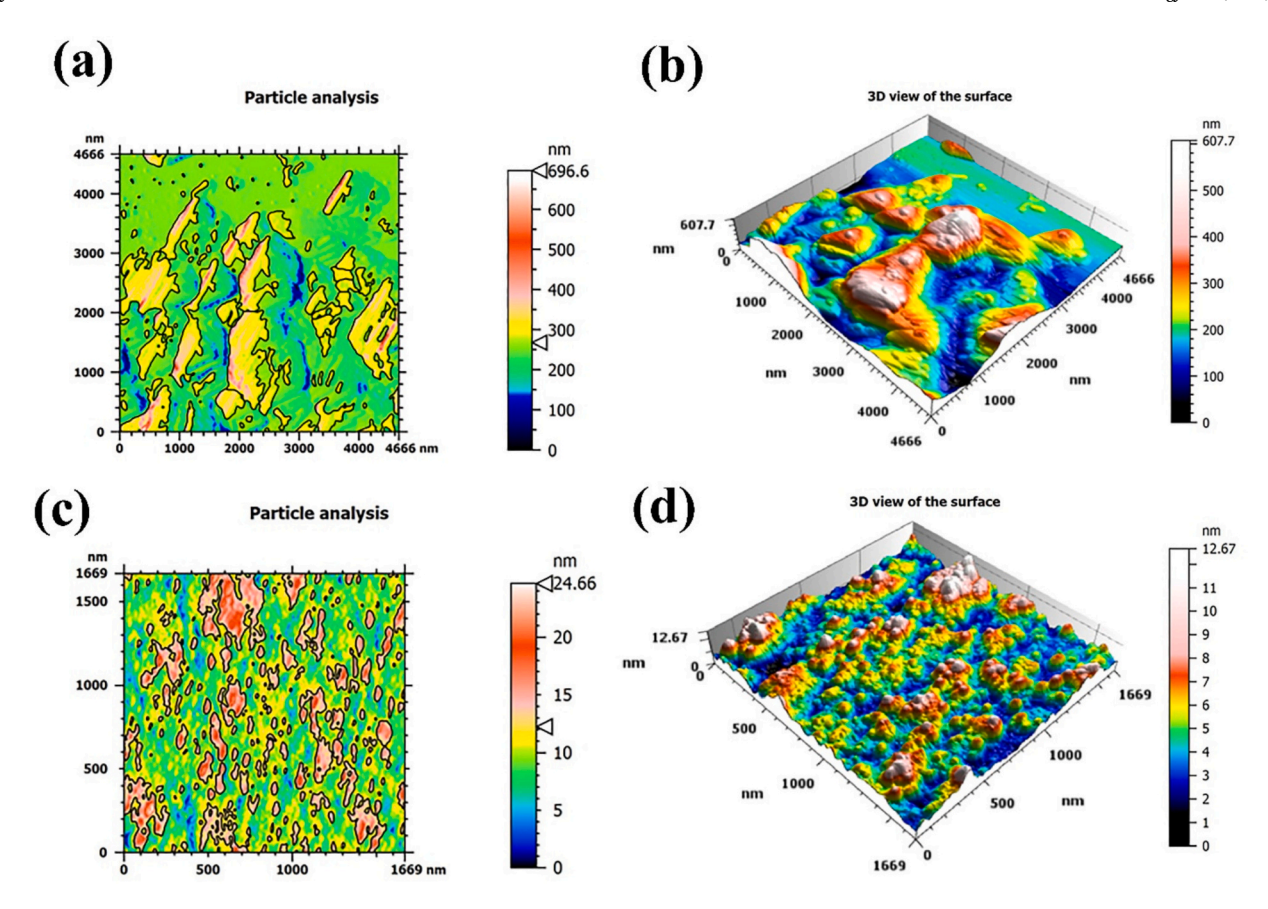


Fig. 2. AFM analysis of micro-bentonite and nano-bentonite. (a) 2D particle analysis of micro-bentonite. (b) 3D view reveals particle sizes of micro-bentonite, (c) 2D analysis of nano-bentonite, (d) 3D view of nano-bentonite.

[26,27].

3.1.2. FTIR analysis of dye adsorption by bentonite in varied water salinities

The FTIR (Fourier Transform Infrared, 1800, Shimadzu, Japan) analysis of Bentonite and Methylene blue dye after removing the dye using Bentonite in both distilled and salty water reveals distinct peaks for each material and environment, indicating different interactions between Bentonite and Methylene Blue Dye. The original Bentonite peaks include 3624 cm⁻¹ and 3442 cm⁻¹ for O-H stretching (hydroxyl groups), 1645 cm⁻¹ for H-O-H bending (water), 1431 cm⁻¹ for C-O stretching (carbonate impurities), 1116 cm⁻¹ and 1037 cm⁻¹ for Si-O stretching (silicate structure), 796 cm⁻¹ for Al-O-Si bending or Si-O-Si bending, and 472 cm⁻¹ for Si-O bending [28,29].

Methylene Blue Dye shows $3400~\rm cm^{-1}$ for stretching of O-H or N-H, $1708~\rm cm^{-1}$ for C=O stretching, $1589~\rm cm^{-1}$ and $1489~\rm cm^{-1}$ for stretching of C=C (aromatic rings), $1394~\rm cm^{-1}$ and $1336~\rm cm^{-1}$ for stretching of C-N (amine groups), $1037~\rm cm^{-1}$ for bending of C-N or C-H; $885~\rm cm^{-1}$ for bending out-of-plane of C-H (aromatic ring); as well as $667~\rm cm^{-1}$ and $447~\rm cm^{-1}$ for stretching of C-S (sulfonic groups) [30].

In the Bentonite-Methylene Blue complex in distilled water, the peaks at 3624 cm⁻¹ and 3419 cm⁻¹ show retention and slight shift of hydroxyl groups, indicating interaction, while 1645 cm⁻¹ and 1602 cm⁻¹ reflect altered C=C stretching vibrations of aromatic rings [31]. The slight shifts at 1390 cm⁻¹ and 1334 cm⁻¹ suggest interactions involving C-N stretching vibrations, and the peak at 1041 cm⁻¹ represents Si-O stretching vibrations with possible interactions. New peaks at 919 cm⁻¹ and 837 cm⁻¹ hint at additional bonding environments, while 796 cm⁻¹ and 470 cm⁻¹ confirm the silicate structure remains largely intact. The peak at 447 cm⁻¹ shows the continued presence of C-S stretching vibrations, indicating interaction with sulfonic groups [22].

The Bentonite-Methylene blue complex in salty water shows peak shifts at 3616 cm⁻¹ and 3433 cm⁻¹, which are due to retention of hydroxyl groups and interactions, as well as characteristics of persistent C=C stretching vibrations of aromatic rings at 1643 cm⁻¹ and 1602 cm⁻¹ [30]. Moreover, the continuous presence of 1334 cm⁻¹ and 1390 ${\rm cm}^{-1}$ indicates similar C-N stretching interactions; other peaks like those at Si-O stretching peaks at 1112 cm⁻¹ and 1033 cm⁻¹ are slightly shifted, indicating weak interaction [31]. Interaction is also indicated by two peaks that have been observed at 837 (Si-OH) and 916(Si-O) cm⁻¹ respectively, in the bentonite structure during contact with distilled water, while the silicate framework remains unchanged after adsorption even with an increased number of new bonding environments subsequently by the addition of Methylene Blue. In fact, according to the FTIR results, all samples show successful adsorption of Methylene Blue onto their surfaces both in distilled water and salty water environments; thus, the indices obtained should be reliable enough for reaching a conclusion on this issue regardless of the saline or distilled type of water used as media. There is shifting or appearance of IR bands particularly those associated with C=C bondings (aromaticity), stretching involving C-N bonds and OH-groups which prove uniform interactions between molecules containing Bentonite surface having dve molecules on it. Salt concentration within the media affects only slightly the interaction mechanism but overall absorption behavior, including bonding remains consistent between both types' aqueous media.

3.1.3. BET, BJH, Langmuir and t plots for micro and nano bentonite

The adsorption isotherms and BET (Brunauer-Emmett-Teller, BEL-SORP MINI II, BEL, Japan) results on μB and nB clearly illustrate how particle size affects the porosity and surface area characteristics of bentonite materials. From Fig. 4(a), nB exhibits a higher volume of gas adsorbed per gram than μB across almost the entire range of relative

pressures, indicating that nB has a more accessible surface area and likely a greater total pore volume, as confirmed by the BET data. This data shows that nB has a pore volume of $0.1302~{\rm cm}^3/{\rm g}$ and a specific surface area of $47.37~{\rm m}^2/{\rm g}$, compared to $\mu B~0.1023~{\rm cm}^3/{\rm g}$ and $36.832~{\rm m}^2/{\rm g}$ respectively, with both materials exhibiting a consistent peak pore size of $1.21~{\rm nm}$. On the other hand, the correlation between void fraction and particle size curves indicates a more efficient packing of pore volumes that are available for adsorption [32]. This improved surface activity is especially useful in applications of catalysis, purification of pollutants, and drug delivery where a higher surface area per unit mass is of great enhancement [33]. Nano-bentonite's increased surface area and pore volume make it more efficient for adsorbing Methylene Blue from water [34]. These characteristics enable it to capture more dye molecules, making it highly effective for water purification applications where removing such contaminants is essential [31].

Fig. 4(b) shows the thickness-dependent sorption capacity for μB and nB reveals that nB consistently exhibits higher sorption capacities across all measured layer thicknesses, outperforming μB . According to the tplot analysis, nB possesses a higher specific surface area of 49.421 m^2/g compared to μB 38.554 m^2/g , indicative of denser surface site packing and more effective molecular adsorption. This enhanced surface area allows nB to excel in applications requiring robust adsorption capabilities, such as environmental remediation and pollutant extraction, by efficiently removing contaminants through both external and internal pore structures [35].

BET study of Micro and Nano bentonite yields the BJH (Barrett-Joyner-Halenda) pore size distribution plot, which gives further pore structure information. Both kinds have peak pore diameters of about 1.21 nm, demonstrating comparable primary pore sizes despite varied particle scales. Nano-bentonite has a bigger area under the curve $(0.1235~{\rm cm}^3/{\rm g})$ than µB $(0.0975~{\rm cm}^3/{\rm g})$, indicating a higher total pore volume. The steeper beginning descent of the nB curve indicates a wider pore size distribution and greater specific surface area $(36.474~{\rm m}^2/{\rm g})$ compared to micro-bentonite $(30.102~{\rm m}^2/{\rm g})$, as shown in Fig. 4(c). Nano-bentonite's wide pore structure and higher surface area make it better for adsorption applications.

As shown in this Fig. 4(d), the novel graph provides detailed adsorption (ADS) and desorption (DES) isotherms for µB and nB with different relative pressures p/p_o . The adsorption curve for μB , plotted with black squares, rises sharply at first before gradually climbing. This may result from the reduced porosity of materials having a small microscale grain size [35]. By contrast, nB has ascending adsorption characterized by blue triangles. This indicates it has a higher adsorption capacity as pressure approaches unity, perhaps due to finer particle size and greater surface area. Both types' desorption curves, given as red circles for micro-and green ones on the Figure for nB, have hysteresis loops, which are typical of this process. That of nB is more marked, indicating a more intricate pore structure and differences on pore connectivity or structural dislocations. Indeed, this whole behaviorparticularly the notably distinct courses for the adsorption curves and desorption ones-demonstrates differences in mesoporous structures between these two materials; where capillary condensation and subsequent evaporation do not follow the same route. As a result of this, the capacity of nB for adsorption and the more pronounced hysteresis circle indicate that it would be most suitable for processes requiring robust adsorption-such as environmental clean-up, or catalysis-because of its larger effective surface area and greater pore volume.

The adsorption behaviors of μB and nB are contrasted in a meaningful way by the Fig. 4(e) that shows P/V_a versus pressure, along with respective Langmuir adsorption constants. The adsorption peak of micro-bentonite is more prominent and occurs at a greater pressure, suggesting that its adsorption capacity is quickly saturated. This is characterized by a Langmuir monolayer adsorption capacity (Vm) of 9.881 cm³(STP) g⁻¹ and a surface area (as, Lang) of 43.007 m²/g. Its Langmuir constant (B) of 0.8588 suggests strong adsorbate-adsorbent interactions, making it ideal for applications where robust and durable

adsorption is necessary. In contrast, the nB which is inclined to the gradual rise then fall in adsorption is effective on a wider range of adsorption at various pressures which can be understood as the effective level of adsorption. It has a higher Vm of 13.204 cm³(STP) g⁻¹ and a larger surface area of 57.47 m²/g but has a B value which is slightly lower, 0.7161 indicating less intense bonding of adsorbate. This profile indicates that the nB is ideal for use in cases where high adsorption capacity is required and where the adsorption has to be flexible due to prevailing conditions in the environment. These specific features show that it is crucial to choose the appropriate type of bentonite depending on the performance requirement for instance if strong adsorption bonding or wide range of adsorption is needed. In the context of adsorption of Methylene Blue from water, it is safe to assume that nB will be more functional than µB. The reason being that nB has a higher $13.204 \,\mathrm{cm}^3$ (STP) g -1 monolayer adsorption capacity, and also a wider surface area 57.47 m²/g, which are both better than those of microbentonite. These factors also illustrate that for each unit mass, nB will be able to dve more than the uB due to increased adsorption sites [30]. Nevertheless, although µB possesses greater adsorbate-adsorbent interactions, as seen with its higher Langmuir constant (B value of 0.8588), the fact that nB can take up a bigger volume of dves before saturation makes it a better material for applications such as wastewater treatment where performance and wide usability are required. Therefore, those qualities of nB make it more appropriate when it comes to the removal and retention of Methylene Blue Dye from physiological solutions.

3.2. Optimization conditions of the adsorption process

Identifying suitable adsorption conditions is crucial for the removal of methylene blue dye to establish a cost-effective adsorption system. The impacts of many parameters were evaluated, including adsorbent dosage, solution pH, agitation time, dye concentration, salt content, and temperature. Various dosages between 0.01 and 0.08 g of each adsorbent (micro and nano bentonite) were introduced to 50 mL of dye solution at a pH of 7, at 25 °C, with an initial concentration of 10 ppm, for 10 min under agitation at 120 rpm. The dye's adsorption effectiveness increases as the adsorbent dosage is increased. For µB, the percentages ranged from 78 % to 88.5 %, and for nB, they ranged from 85 % to 92 %. The adsorbent's enhanced surface area availability at higher concentrations and the dye ions' full utilization of all active sites account for the improvement in adsorption effectiveness [36]. Increasing the amount of adsorbent above 50 mg for μB and 30 mg for nB doesn't have a big effect on how well it removes the substance. This is because the adsorbent (solid) and adsorbate (liquid) are already in equilibrium [37]. This is due to the finite number of active binding sites on each adsorbent, making it increasingly difficult to occupy these sites with dye over time [38]. Therefore, we selected adsorbent dosages of 50 mg and 30 mg as the optimal amounts to achieve maximum dye adsorption efficiencies of 88 % and 91 % for µB and nB, respectively, as is shown in Fig. 2a. We altered the pH of the dye solution at values of 2, 4, 6, 8, and 10 to examine its impact on the percentage of dye removal. Fig. 2b illustrates how pH affects the adsorption efficiency of μB and nB in dye solutions. We performed the studies at the optimal adsorbent doses. The dye removal efficiencies diminish as the pH value rises, achieving maximum removal efficiencies of 93 % and 95 % for µB and nB, respectively, at a pH value of 2. The removal efficiency diminished at pH greater than 2 due to electrostatic interactions between Ca2+ ions on bentonite and dye; acidic pH provides more adsorption sites on the adsorbent for dye removal compared to alkaline pH [39]. We assessed the impact of shaking duration over time intervals ranging from 10 to 60 min at the optimal adsorbent dosage and pH value. After 40 min of shaking, the removal efficiency increased from 88 % to 93.5 % for μB and from 90.5 % to 95.5 % for nB, as shown in Fig. 4c. The adsorption efficiency stabilized with time due to the repulsion of solute molecules and bulk phases, resulting in the saturation of active sites [40]. We established the

ideal shaking duration of 40 min for each adsorbent. Furthermore, elevating the concentration of the dye pollutant from 5 to 25 ppm enhanced the efficacy of μB in its removal (90–96.36 %) and improved the performance of nB (93-97.24 %) at optimal dosage, pH, and agitation duration, as illustrated in Fig. 4d. Removing contaminants at low concentrations is more challenging than at high concentrations for the following reasons: First, The driving force for mass transfer is low. At high concentrations, the difference between the concentration of the contaminant in the solution and the surface of the adsorbent is large, increasing the rate of migration of molecules toward the surface. While, at low concentrations, this driving force decreases, and thus the adsorption rate is slower. Thereby, at low concentrations, materials with a large surface area and numerous active sites are required to increase the potential for trapping molecules [39,41,42]. Second, through the relationships between adsorption efficiency and capacity (Eqs. (1) and (2)), it is clear that the increase in the difference between the initial and residual concentration of the contaminant is directly proportional to both the adsorption capacity and efficiency. For the reasons mentioned, relatively low concentrations were selected due to the challenge they pose.

[43] utilized multiple kinetic models, including Pseudo First Order (PFO), Pseudo Second Order (PSO), Elovich (Elo), and Intra Particle Diffusion (IPD) models, to rigorously analyze the adsorption rate and the rate-limiting step. Eq. (3) quantitatively demonstrates the premise of the PFO kinetic model, which asserts a direct correlation between the rate of adsorption site occupancy and the number of vacant sites. This method is especially advantageous for analyzing the occupancy dynamics of adsorption sites [44]. Moreover, Inyinbor, Adekola, and Olatunji [45] clarify that the adsorption capacity of the adsorbent dictates the linear representation of the PFO model, as articulated in Eq. (4). These kinetic models provide critical insights into the dynamics of the adsorption process. They identify the rate-limiting phases and provide a comprehensive overview of the adsorption mechanisms relevant to the researched materials and systems.

$$qt = qe\left(1 - e^{-k_I^t}\right) \tag{3}$$

$$ln\left(qe-qt\right)=lnqe\text{-}k_{I}t\tag{4}$$

Eq. (5) [46] illustrates the correlation between the rate of adsorption site occupation and the square of the active adsorption sites when utilizing the adsorption kinetic models of Pseudo Second Order (PSO). This model provides substantial insights into the temporal progression of adsorption site occupancy. [47] provide the equation governing the PSO model, based on the adsorption capacity of the solid phase, presented in a linear fashion as Eq. (6). This model associates the kinetic rate with the accessibility of active sites, providing a clear comprehension of adsorption kinetics and improving the understanding of the mechanisms and dynamics of adsorption in the studied system.

$$qt = qe\left(1 - \frac{1}{1 + k2t}\right) \tag{5}$$

$$\frac{t}{qt} = \frac{1}{k2qe2} + \frac{t}{qe} \tag{6}$$

The Elovich model is a prevalent framework for characterizing adsorption processes, notably recognized for its capacity to clarify situations where the adsorbate persists on the solid surface without desorption. This model suggests that the adsorption rate decreases with prolonged contact time between the adsorbate and adsorbent. This effect is attributed to the gradual rise in surface coverage over time. In 2015, De La Luz-Asunción et al. expanded on this idea, highlighting the crucial importance of the Elovich model in clarifying the intricate nature of adsorption mechanisms [43]. This model offers essential insights into the dynamic properties of adsorption processes by suggesting a continual accumulation of adsorbate on the solid surface. It clarifies the

changes in surface interactions as the system develops. Asnaoui and his team delineate the equations for the nonlinear and linear Elovich kinetic models [48].

$$qt = \beta \ln(\alpha \beta t) \tag{7}$$

$$qt = 1/\beta \ln(\alpha\beta) + 1/\beta \ln(t)$$
(8)

In this context, q_t represents the quantity of adsorbate adsorbed at time t (mg/g), α denotes a constant associated with the rate of chemisorption, and β signifies a constant that illustrates the degree of surface covering. Additionally, k_1 (min - 1) and K_2 (mg/g/min) are the rate constants for the pseudo-first-order (PFO) and pseudo-second-order (PSO) kinetics, respectively.

The Intra Particle Diffusion model is employed to examine the diffusion-controlled adsorption system. A linear fit suggests that the adsorption process involves the dispersion of many stages. Intra Particle Diffusion constitutes the sole rate-limiting step if the plot intersects the origin. The Weber-Morris model equation is articulated as follows [5]:

$$qt = k_{id}t^{0.5} + \theta \tag{9}$$

In this context, k_{id} represents the Intra Particle Diffusion rate constant (mg/g min^{0.5}), whereas θ signifies a constant that denotes the thickness of the boundary layer (mg/g).

The adsorption capacity, defined as the quantity of dye adhering to a single unit of adsorbent, must be graphed versus agitation time (t) to illustrate the adsorption kinetic curves for each adsorbent [49]. Fig. 3 visually illustrates this process; using the meticulously documented experimental data in Table 2, we employ linear Eqs. (4), (6), (8), and (9) to determine the characteristic constants of each kinetic model and adsorbent. This research demonstrates a notable trend: the correlation coefficients (R²) for the adsorbents linked to the pseudo-second-order kinetic model are much higher than those derived from alternative kinetic models. This conclusion is crucial, as the R² values quantitatively assess the degree of correspondence between the theoretical models and the experimental outcomes [50]; [51]. This study compares different adsorbents and shows that the pseudo-second-order kinetic model is better at predicting how the dye will be absorbed. The higher value of R² achieves in this model means that the predictions and the results of the experiments are more closely aligned, which leads to more accurate and reliable kinetic interpretations. Detailed research like this one shows how dye adsorption changes over time and helps choose the best kinetic

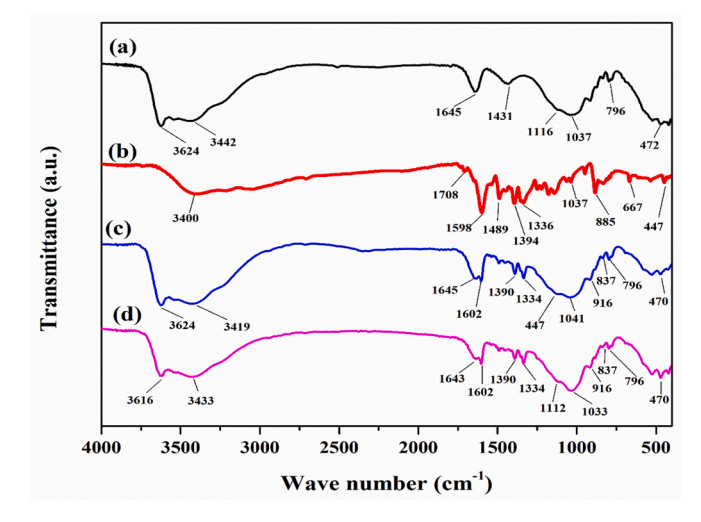


Fig. 3. FTIR spectra of Bentonite and Methylene Blue Dye. (a) Pure Bentonite, (b) Methylene Blue Dye, (c) Methylene Blue removed by Bentonite in distilled water, and (d) Methylene Blue removed by Bentonite in salty water. (For interpretation of the references to colour in this figure legend, the reader is referred to the web version of this article.)

Table 2The parameters of adsorption kinetic models to remediate methylene blue dye utilizing the adsorbents of bentonite and Nano bentonite at optimal conditions.

Model	Parameters	Bentonite	Nano Bentonite	
Pseudo first order	K1	0.1199	0.1151	
	\mathbb{R}^2	0.9624	0.9499	
Pseudo second order	K2	0.145	0.0926	
	R^2	1.000	1.000	
Elovich	α (mg/g.mint)	3.189039×10^{10}	1.123144×10^{12}	
	β (g/mg)	3.11915	2.0296	
	R^2	0.9132	0.9209	
Intra Particle	Θ(mg/g)	8.5284	14.645	
Diffusion	K _{id} (mg/g. min ^{0.5})	0.1191	0.8138	
	R^2	0.8298	0.8439	

model to explain and predict the complex adsorption behavior of the tested adsorbents.

To describe the adsorption isotherm curves for each adsorbent, you need to plot the adsorption capacity (qe) against the concentration of the remaining dye (Ce). Fig. 4 shows how this graphical method lets us compare experimental dye adsorption data with three main theoretical adsorption isotherm models: Langmuir, Freundlich, and Tempkin. The Langmuir isotherm model, as explained by Eqs. (3) and (4) [52], is one of adsorption science's fundamental models, postulates the formation of a monolayer of adsorbate on a homogeneous adsorbent surface [53]. Researchers employ the Langmuir isotherm to clarify the surface properties of the adsorbent, the interactions among adsorbate molecules, and the available sites [54]. Researchers ascertain the most precise correlation by juxtaposing experimental data with theoretical models, thus identifying the isotherm that most accurately represents the adsorption

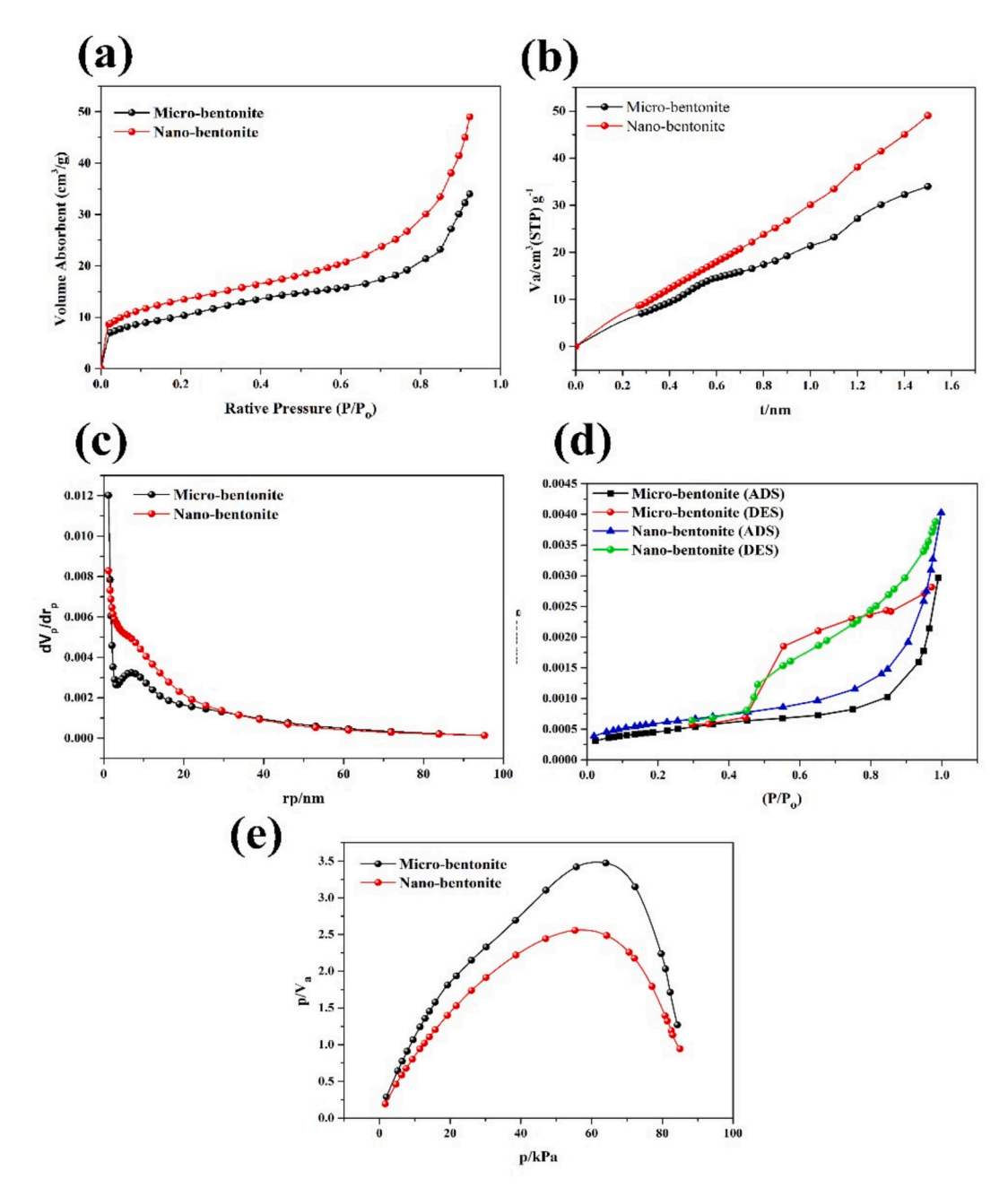


Fig. 4. (a) BET adsorption isotherms of Micro-bentonite and Nano-bentonite, (b) T-plot sorption capacity of Micro and Nano Bentonite as a function of layer thickness, (c) BJH pore size distribution of Micro and Nano bentonite, (d) Adsorption (ADS) and Desorption (ABS) isotherms for micro nano bentonite and (e) The P/ V_a versus pressure (p) graph for micro and nano bentonite showing Langmuir adsorption behaviors.

process under investigation [55]. A comprehensive analysis such as this elucidates the interaction between adsorbent surfaces and adsorbate molecules. It establishes a robust foundation for subsequent enhancements and applications of adsorption techniques (refer to Fig. 4).

$$qe = (Q \times K_L \times Ce)/(1 + K_L Ce)$$
(10)

$$Ce/qe = Ce/Q + 1/(Q \times K_L)$$
(11)

(See Figs. 5-7.)

 Q_0 signifies the maximum monolayer coverage and capacity (mg/g), whereas K_L represents the Langmuir isotherm constant (L/mg). The Freundlich isotherm model exemplifies an empirical approach that accommodates multilayer adsorption processes, rather than merely depicting a single layer of coverage [56]. This model is particularly efficacious for adsorption situations on heterogeneous surfaces where the distribution of active sites and their corresponding energy adhere to an exponential pattern. [37] mathematically articulate the Freundlich isotherm to describe the correlation between the amount of adsorbate absorbed and its equilibrium concentration in the adsorbent. This empirical model effectively demonstrates multilayer adsorption, rendering it valuable for illustrating real adsorption systems where several adsorbate molecules accumulate on the adsorbent's surface [57]. The Freundlich isotherm elucidates the variations in adsorptive behavior within intricate, heterogeneous environments by considering the distribution of active sites and their interactions with diverse substances [58].

$$q_e = K_F C_e^{1/n} \tag{12}$$

$$\log q_e = \log K_E + 1/n \log C_e \tag{13}$$

In this context, K_F represents the Freundlich constant associated with sorption capacity, whereas 1/n indicates the degree of sorption.

The Tempkin isotherm model can be written as the following form [14]:

$$q_e = RT/b(lnAC_e)$$
 (14)

$$q_e = (RT/b)lnA + (RT/b)lnC_e$$
 (15)

$$B = RT/b \tag{16}$$

B represents the heat of adsorption, R denotes to the ideal gas constant (8.314 J/mol·°K), T (°K) signifies the absolute temperature at 298.15 K, b is the Temkin isotherm constant, and A (L/g) indicates the equilibrium binding constant associated with the maximal binding energy. We derived the parameters for each model and adsorbent from the nonlinear equations, employing the experimental data presented in Table 3. The plethora of vacant sites for adsorption and the existence of functional groups that promote dye adsorption from an aqueous solution likely enhance the initial adsorption rates. Subsequently, the saturation of adsorption sites results in a reduction in the dye solution concentration until equilibrium is attained [59]. The increase of surface area, pore volume, and functional groups enhanced adsorption capacity, leading to an increase from 24.05 to 40.33 mg/g for µB and nB, respectively [60]. The findings indicate that the Freundlich isotherm better correlates with the experimental data compared to the Langmuir and Tempkin adsorption isotherms for the removal of methylene blue dve across all adsorbents, as evidenced by the correlation coefficient R² values [61] (see Table 3).

To explain the effect of temperature change on the adsorption process, thermodynamics curves and parameters for each adsorbent were studied. The plots indicate the relationship between the equilibrium

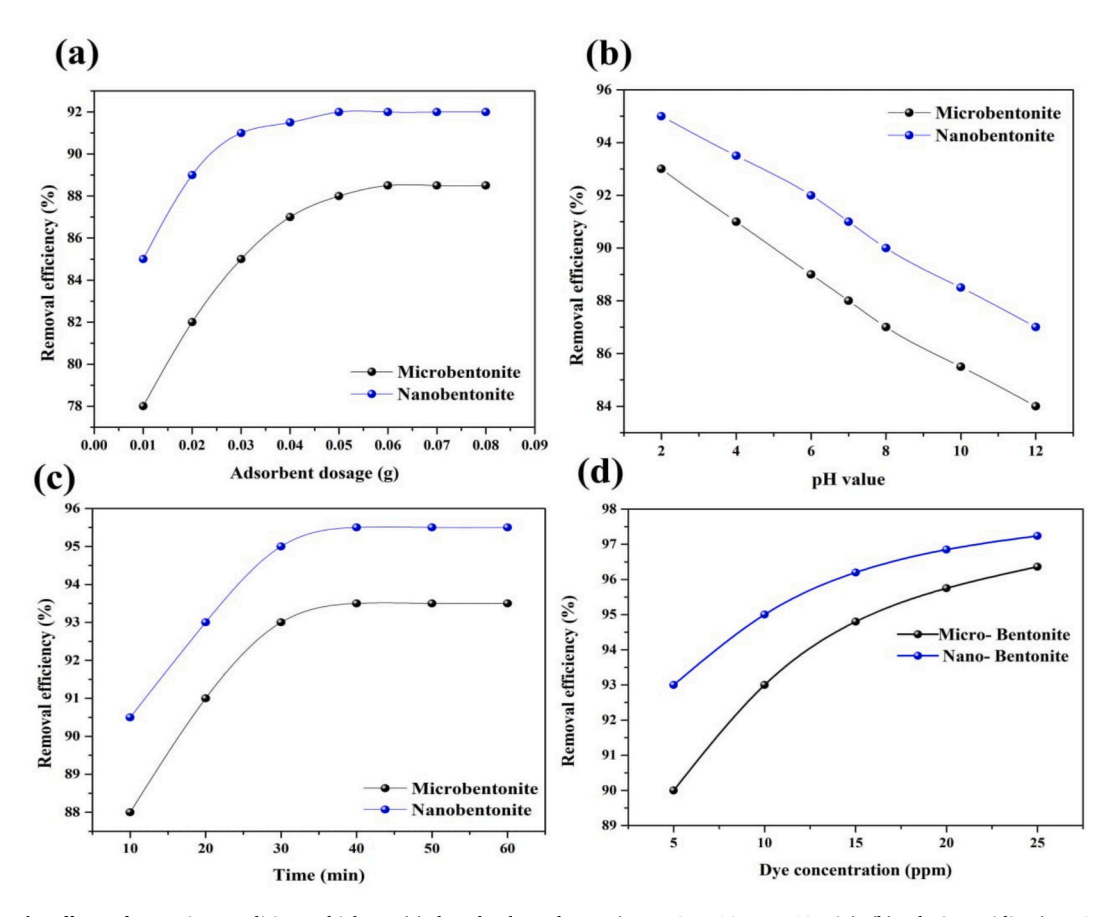


Fig. 5. Represent the effects of operating conditions which are (a) the adsorbent dosage (pH 7, $C_0 = 10$ ppm, 10 min); (b) solution acidity (μ B 50 mg and nB 30 mg, $C_0 = 10$ ppm, 10 min); (c) agitation time (pH 2, μ B 50 mg and nB 30 mg, $C_0 = 10$ ppm); (d) initial dye concentration (pH 2, μ B 50 mg and nB 30 mg, 40 min).

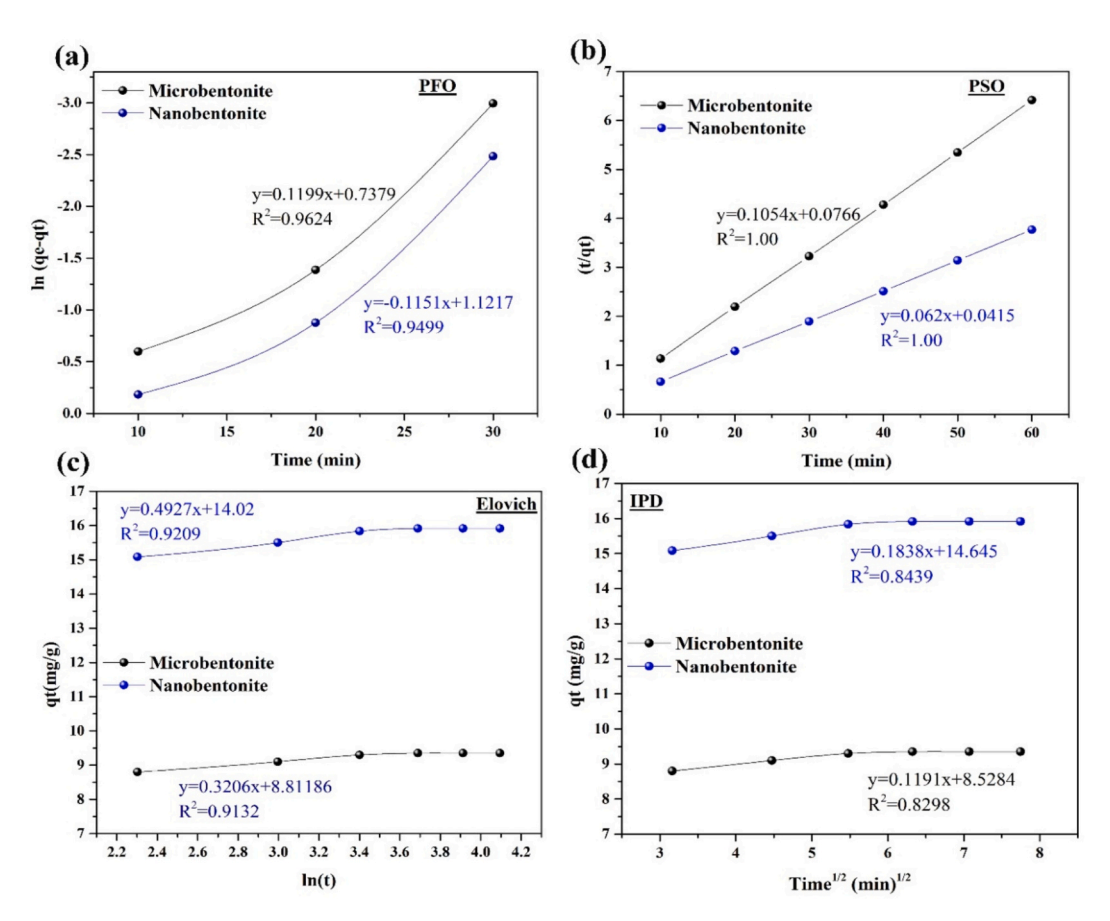


Fig. 6. Represent the kinetic adsorption models for micro and nano-bentonite.

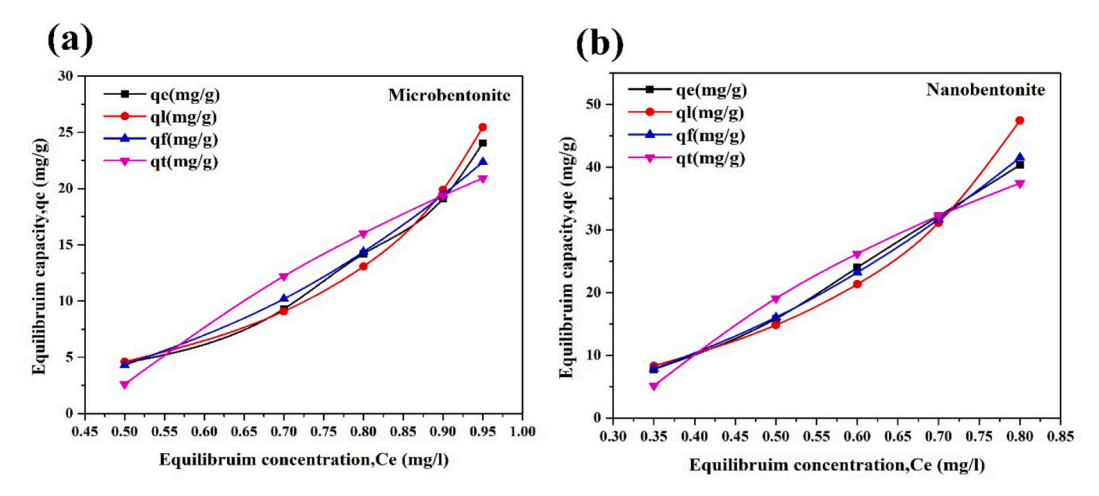


Fig. 7. Represent the adsorption isotherm models for micro and nano-bentonite.

constant (K) and the reciprocal temperature (1/T) as showed in Fig. 8. The parameters concluded from Eqs. (17)–(20) and the linear equation extracted from Fig. 8a, including the values of changes in enthalpy ($\Delta H^{\circ} = -\text{slope/R}$) and entropy ($\Delta S^{\circ} = \text{intercept/R}$), were used to calculate the free energy of sorption (ΔG°) [62–64], as illustrated in Table 4.

$$K = qt/Ce$$
 (17)

$$\Delta G^{\circ} = -RT \ln K \tag{18}$$

$$lnK = \Delta S^{\circ}/R - \Delta H^{\circ}/RT$$
 (19)

$$\Delta G^{\circ} = \Delta H^{\circ} - T\Delta S^{\circ} \tag{20}$$

The assessment of thermodynamic parameters is crucial for analyzing spontaneity and thermal changes in adsorption reactions. The negative values of ΔG° validate the process's viability and the spontaneous nature of adsorption. On the other hand, the more negative number associated with a rise in temperature signifies that enhanced adsorption is achieved at elevated temperatures. The positive values of ΔH° corroborated the endothermic nature of adsorption, further evidenced by the enhanced pollutant uptake of the adsorbent with increasing temperature. The positive values of ΔS° indicated heightened

Table 3The parameters of adsorption isotherm models to remediate methylene blue dye utilizing the adsorbents of bentonite and nano bentonite at optimal conditions.

Model	Parameters	Bentonite	Nano Bentonite
Langmuir	$Q_0 (mg/g)$	-6.293	-17.762
	$K_L (L/mg)$	-0.844	-0.9095
	R^2	0.9798	0.9842
Freundlich	1/n	2.5723	2.0222
	K_{f}	25.5035	65.1928
	\mathbb{R}^2	0.9848	0.993
Tempkin	$A_T (L/g)$	2.1908	3.2579
	b_{T}	86.777	63.3779
	B (J/mol)	28.551	39.092
	R^2	0.9052	0.9241

randomness at solid/solution interfaces during adsorption and increases in state of randomness in the molecules throughout the process [62–65].

As showed in Table 4 the results demonstrate that nano-bentonite typically had superior thermodynamic characteristics relative to micro-bentonite, attributable to its increased active sites and enhanced binding affinity, which produce larger interfacial disorder during adsorption. Their surface energy and reactivity markedly increase the spontaneity of adsorption [66–68].

Determination of activation energy (Ea) is a crucial parameter in chemical kinetics, indicating the minimum energy necessary for a reaction or adsorption event to occur. The magnitude of Ea in adsorption studies offers important clues about the nature of the adsorption process. Physisorption is primarily influenced by weak van der Waals forces and demonstrates activation energies in the range of 5–40 kJ/mol. Chemisorption, in contrast, entails the formation of chemical bonds and necessitates considerably higher energies, ranging from 40 to 800 kJ/mol [69]. Pseudo second order was used to evaluate the kinetic constant (K_T) at different temperature ranange (25–55 °C) for micro and nano adsorbents as showed in Figs. 9 and 10 respectively. [70] The calculated values based on the Arrhenius Eqs. (21) and (22) are 13.54 kJ/mol for nano-bentonite and 15.25 kJ/mol for micro-bentonite as showed in

Fig. 11. The values align with the anticipated range for physisorption, suggesting that the process is primarily governed by weak physical interactions instead of chemical bonding. The reduced activation energy of the nanomaterial indicates improved adsorption efficiency, attributed to its increased surface area, shorter diffusion pathways, and the presence of numerous active sites that promote adsorption with minimal energy barriers. The observed Ea values confirm that the adsorption mechanism is physisorption.

$$K_{T} = A e^{Ea/RT}$$
 (21)

$$Ln (K_T) = ln(A) - Ea/RT$$
 (22)

(See Figs. 12 and 13.)

3.3. Mechanism of adsorption

The activation energy (Ea) for adsorption was determined to be low, at 13.54 and 15.25 kJ/mol for nano and micro bentonite, respectively. This suggests that the process is physisorption, as it is generally associated with activation energies below 40 kJ/mol and involves weak van der Waals interactions between the adsorbate and the adsorbent surface [71]. Kinetic analysis indicated that the pseudo-second-order (PSO) model exhibited the highest correlation (R² values approaching unity), implying that the adsorption process is primarily influenced by the availability of active sites on the adsorbent surface, rather than being regulated by external mass transfer or intra-particle diffusion. This suggests that while the adsorption process is primarily physical, the overall rate is notably affected by the interactions between adsorbate molecules and the heterogeneous surface of the adsorbent [41]. Equilibrium data were most accurately represented by the Freundlich isotherm model, indicating that adsorption takes place on a heterogeneous surface characterized by sites with varying affinities, facilitating multilayer adsorption. The Freundlich constant (n) further validated the favorable nature of the adsorption process, indicating the adsorbent's effectiveness in removing the target species [72]. The adsorption

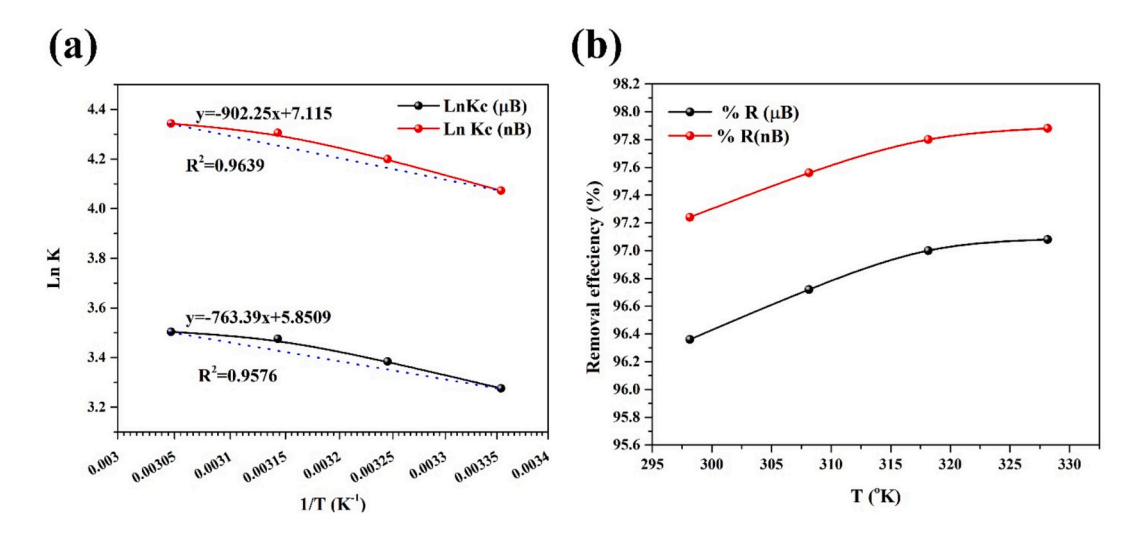


Fig. 8. Represent a- thermodynamic curves for micro and nano bentonite and b- effect of temperature changes on the removal efficiency at optimum adsorption conditions.

Thermodynamic parameters for micro and nano bentonite at optimum conditions.

orbent	Ln Kc			ΔH° ΔS°	ΔG°(KJ/mol.)					
	25 °C	35 °C	45 °C	55 °C	(KJ/mol.)	(KJ/mol.°K)	25 °C	35 °C	45 °C	55 °C
μB -B	3.28	3.39	3.48	3.50	6.35	0.049	-8.16	-8.64	-9.13	-9.62 -11.91
nB	4.07	4.20	4.31	4.34	7.50	0.059	-10.14	-10.73	-11.32	

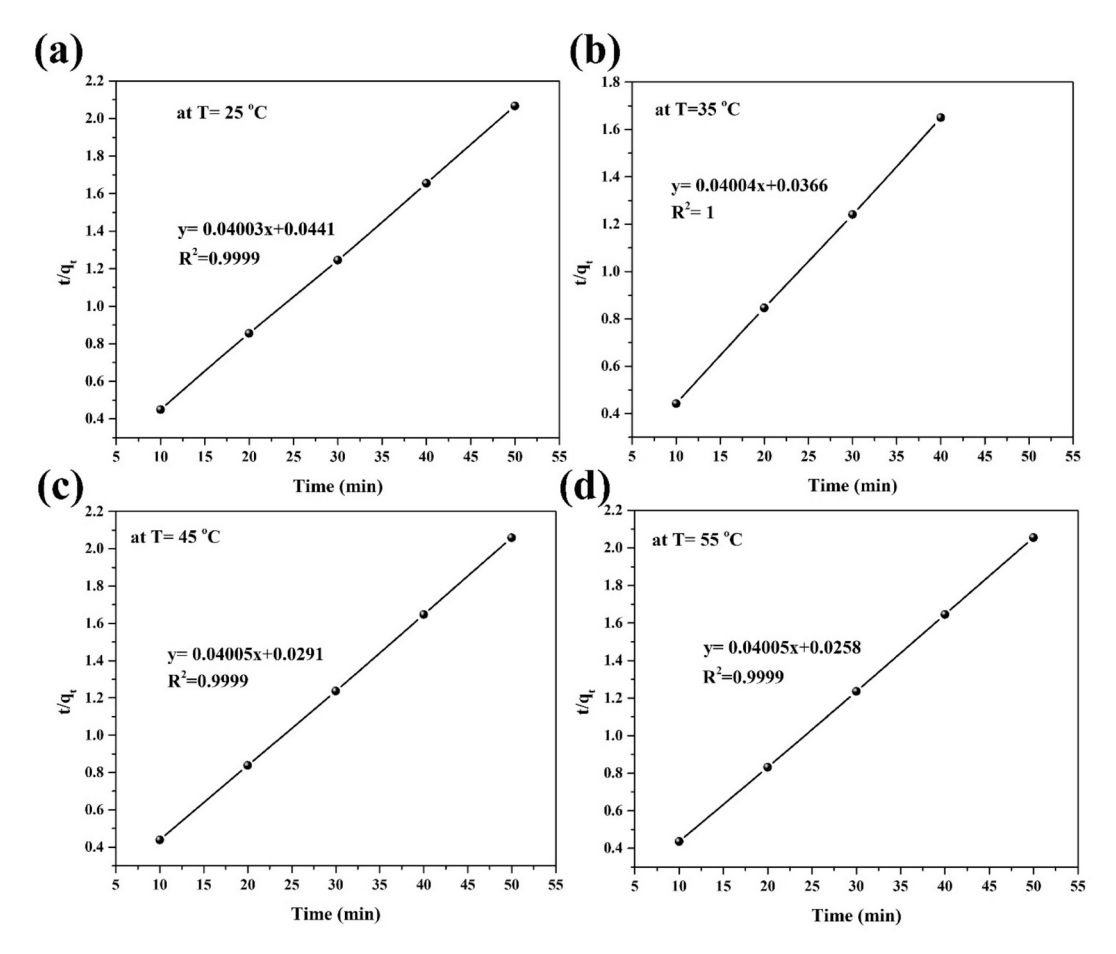


Fig. 9. Pseudo second order to calculate the kinetic constants (K_T) at temperature range (25–55 °C) for micro-bentonite at optimum adsorption conditions.

mechanism is characterized by physisorption on a heterogeneous surface, with kinetics adhering to a pseudo-second-order model. The equilibrium data align with the Freundlich model, suggesting multilayer adsorption at sites with varying energy levels.

3.4. Disposal methods for spent bentonite adsorbent containing methylene blue dye

The management of spent bentonite adsorbents contaminated with blue dye necessitates strategies that ensure both environmental safety and practical feasibility. Thermal treatment, such as calcination at temperatures ranging from 250 to 450 °C, effectively decomposes the dye while maintaining the integrity of the clay, thus allowing for reuse in future applications or safe inert disposal [70]. Alternatively, chemical regeneration employing oxidizing agents like H₂O₂ under UV irradiation has demonstrated the complete restoration of adsorption capacity in magnetic bentonite composites [73]. Solvent-mediated regeneration, such as with ethanol or acid solutions, facilitates multiple reuse cycles prior to disposal [74]. If regeneration models are deemed impractical, solidification and stabilization through cementitious matrices effectively immobilize the dye-clay complex, thereby minimizing environmental release and complying with hazardous waste stabilization standards (cement remediation protocols). These strategies effectively ensure the safe and sustainable management of spent bentonite.

3.5. Salt effects

Water contaminated by diverse industrial activities typically contains different concentrations of salts or is released into saline water. Consequently, the influence of salt content on the adsorption process

was examined to enhance the research's global dependability. A sample of water was collected from the renowned Shatt Al-Arab river in Basra Governorate. We evaporated it to extract salt and utilized it in varying dosages from 0.05 to 0.5 g, added to a 50 mL aqueous solution contaminated with dye under ideal conditions. Table 5 presents the characteristics of saline water contaminated with dye, as determined by a TDS meter (HANNA HI98192, Romania).

The results indicate that the adsorption capability is unaffected by salt concentrations ranging from 1000 to 10,000 ppm (0.017-0.17 molarity). Various physicochemical factors contribute to bentonite's insensitivity to elevated salinity (up to 10,000 ppm) regarding its adsorption efficacy for organic dyes. The stability of bentonite's surface charge stability under moderate ionic strengths owing to its negatively charged layer and elevated cation exchange capacity (CEC). Exchangeable cations in bentonite interlayers, including Na⁺, Ca²⁺, and Mg²⁺, might mitigate the impact of external salts, hence decreasing the probability of competitive ion exchange with dye molecules. The adsorption of organic dyes, such as methylene blue, onto bentonite is governed by mechanisms beyond mere electrostatic attraction, notably the predominance of π - π interactions and other influences. Supplementary processes, such as hydrogen bonding, π - π stacking, and van der Waals interactions, significantly contribute. These techniques maintain their adsorption efficacy even when subjected to moderate salt concentrations [75]. The ionic strength of NaCl, which can attain levels of up to 10,000 ppm (~0.17 M), is inadequate to fully screen the surface charges of bentonite or to disturb the interactions between the dye and the surface. The literature demonstrates that the adsorption rate is markedly diminished due to electrostatic screening and competition solely at considerably elevated salinity levels (>0.5–1.0 M). The hydrophobicity of the dye and steric hindrance arise from aromatic planar structures

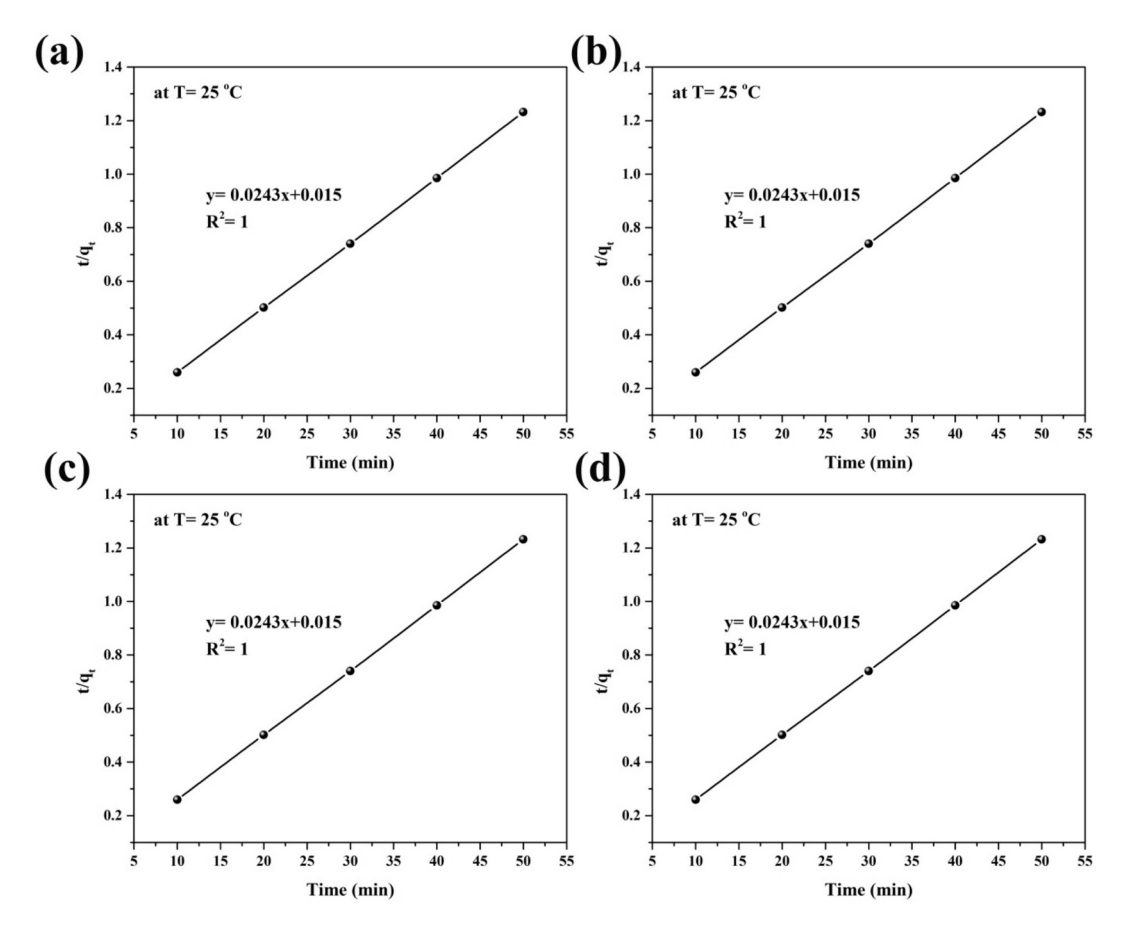


Fig. 10. Pseudo second order to calculate the kinetic constants (K_T) at temperature range (25–55 $^{\circ}$ C) for nano-bentonite at optimum adsorption conditions.

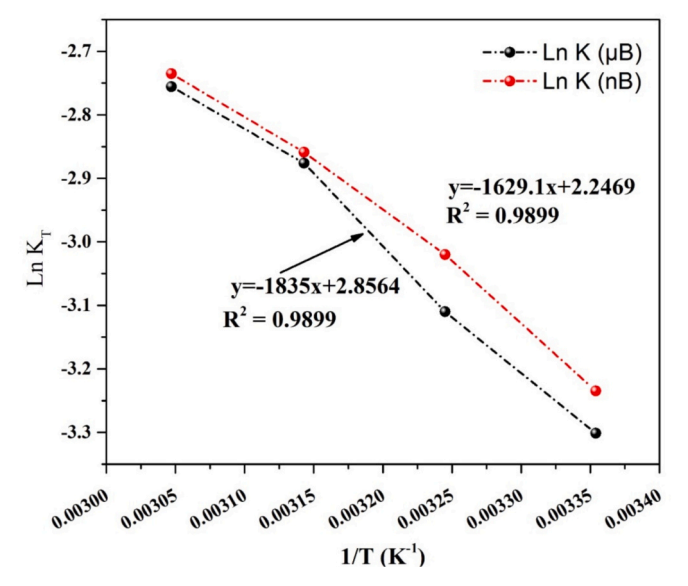


Fig. 11. Represent the linear equations to calculate the activation energy for micro and nano-bentonite at optimum adsorption conditions.

containing hydrophobic domains. Due to their minuscule size and high solubility, salt ions cannot displace dye molecules off a surface once they have occupied an adsorption site. Consequently, the adsorption capacity remains mostly unchanged. The ability of bentonite to expand in saline conditions renders it an optimal material for dye intercalation due to the formation of accessible interlayer spaces. This structural attribute alleviates the competitive impact of dissolved salts [66].

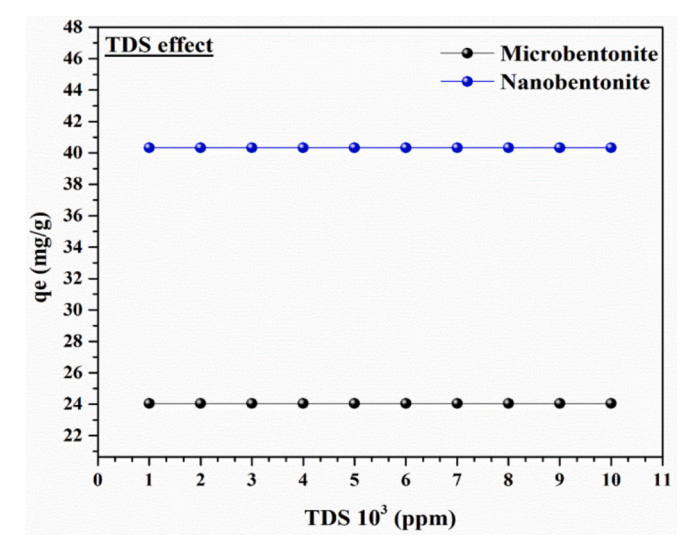


Fig. 12. Salt effects on the adsorbent capacity.

3.6. Adsorbent stability (reusability)

The adsorption of dye molecules from the adsorbent surface improves its reusability. The adsorption of methylene blue was minimal when the process occurred at a pH of twelve, as indicated by the pH studies. At alkaline pH, the adsorbed M.B. molecules can be desorbed from the adsorbent. In accordance with these findings, the M.B.-loaded adsorbent was desorbed utilizing 0.1 M NaOH. Before collection, we stirred the mixture for 4 h at 25 $^{\circ}$ C, washed it with distilled water, and

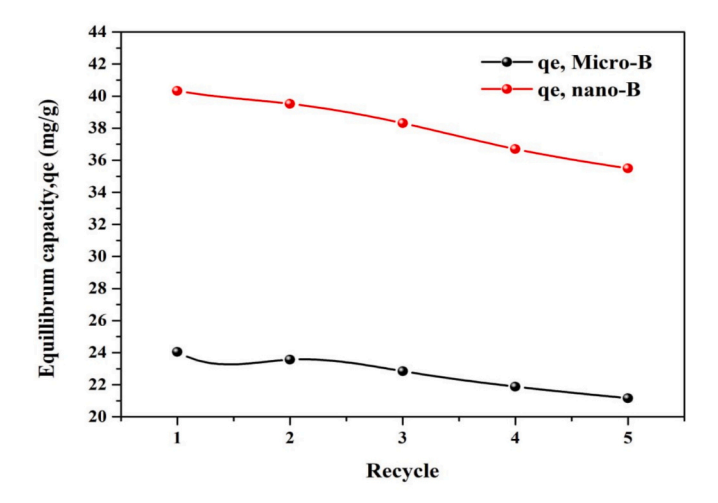


Fig. 13. Showing the adsorption stability for micro-B and nano-B.

Table 5
Shows the salt concentrations and its related properties of the dye polluted solution

$\text{TDS} \times 10^3 \text{(ppm)}$	$\times 10^3$ (ppm) Salt (PSU)		Resistivity (Ω)	
1	1.21	2.373	421	
2	2.25	4.271	234	
3	3.34	6.180	162	
4	4.46	8.095	123	
5	5.64	10.06	99.3	
6	6.18	11.01	90.8	
7	7.22	12.74	78.5	
8	8.52	14.84	67.4	
9	10.27	17.63	56.7	
10	11.29	19.23	52.0	

dried the adsorbent for later use. After five cycles, the adsorption capacities of μB and nB retained at least 85 % and 87 % of them. initial values, respectively, as illustrated in Fig. 8.

3.7. Process cost evaluation

The creation of nanoparticles using ball milling is distinguished by its scalability and cost-effectiveness when compared to alternative synthesis approaches. It obviates the necessity for detrimental solvents and costly precursors. This approach is applicable to many adsorbents. The principal expenditures encompassed the ball mill equipment, liners, and grinding medium. Operating expenses encompass electricity consumption, maintenance, and the deterioration of balls. Anticipated energy consumption varies between 15 and 50 kWh per ton of material, contingent upon characteristics such as hardness and target dimensions [76]. The production of the adsorbent involves costs associated with raw ingredients and the grinding procedure. Expenditures associated with regeneration and reuse can be classified as either thermal or chemical [77]. Nanoparticles typically have improved adsorption capacity (qe) and expedited kinetics, leading to reduced adsorbent dosage and abbreviated treatment period. The reduction in preparation costs of microparticles results in lower adsorption efficacy, necessitating greater material consumption and prolonged contact duration.

4. Conclusions

The treatment of wastewater is critical because of the environmental and public health hazards it presents. The recovery process and adsorbents' limited adsorption capacity, both due to organic pollutants, present significant challenges. This work aimed to enhance bentonite for wastewater treatment by reducing the adsorbent particle diameter to

increase surface area and pore volume through a straightforward physical treatment procedure, achieving a nanoscale dimension. Beyond routine experimental work, this study advances the field by demonstrating the stability of bentonite adsorption under saline conditions, the superior performance of nano-bentonite, and the practical reusability of the adsorbent, key innovations that enhance its applicability in industrial wastewater treatment. The two M.B. dve adsorbents-Micro and Nano bentonite—exhibit a stunning 99.926 % efficiency in M.B. dye removal. The batch adsorption experiments revealed a correlation between adsorbent dosage and dye removal, peaking at 0.05 g for microbentonite and 0.03 g for nanobentonite. These adsorbents demonstrated their effectiveness at an ideal pH of 2 and a constant temperature of 25 °C. As time progressed, the dye adsorption efficiency exhibited a progressive increase until reaching equilibrium, peaking around 40- min for both micro- and nanobentonite. The experimental results in the kinetic domain aligned with the Pseudo Second Order (PSO) model, exceeding the performance of alternative kinetic models. The Freundlich isotherm was a better model of the sorption isotherm than the Langmuir and Tempkin models because it fit the experimental data better. Moreover, their reusability without discernible capacity degradation presents substantial potential for practical application in the removal of M.B. dye from water. This research shows how important adsorbent loading, contact duration, pH, and isotherm models are for making nanobentonite better at removing M.B. dye. We examined an essential issue that most prior studies overlooked, specifically the impact of salts on adsorption efficiency. We determined that salts do not influence the efficiency of adsorption for concentrations ranging from 10³ to 10⁴ ppm. Subsequent research may refine the synthesis technique to enhance adsorption capabilities and efficiency and explore possible scale-up methodologies for practical wastewater treatment applications.

CRediT authorship contribution statement

Hassan Wathiq Ayoob: Resources, Methodology. Nabil Kadhim Taieh: Investigation, Formal analysis, Data curation. Abdulrazzaq S. Abdullah: Supervision, Project administration. Raad Z. Homod: Conceptualization. F. Medina: Writing – original draft, Visualization.

Declaration of competing interest

The authors declare that they have no known competing financial interests or personal relationships that could have appeared to influence the work reported in this paper.

Data availability

No data was used for the research described in the article.

References

- [1] F.M.S.E. El-dars, H.M. Ibrahim, H.A.B. Farag, M.Z. Abdelwahhab, M.E.H. Shalabi, Using bentonite carbon composite material for adsorption of bromocresol purple and methylene blue, Int. J. Sci. Eng. Res. 6 (10) (2015) 188–197.
- [2] R. Al-Tohamy, et al., A critical review on the treatment of dye-containing wastewater: ecotoxicological and health concerns of textile dyes and possible remediation approaches for environmental safety, Ecotoxicol. Environ. Saf. 231 (2022) 113160. https://doi.org/10.1016/j.ecoenv.2021.113160.
- [3] S. Dardouri, J. Sghaier, Adsorptive removal of methylene blue from aqueous solution using different agricultural wastes as adsorbents, Korean J. Chem. Eng. 34 (4) (2017) 1037–1043, https://doi.org/10.1007/s11814-017-0008-2.
- [4] E. Alver, F. Brouers, International Journal of Biological Macromolecules Methylene blue adsorption on magnetic alginate / rice husk 154 (2020) 104–113, https://doi. org/10.1016/j.ijbiomac.2020.02.330.
- [5] C.O. Aniagor, A.A. Aly, L.A. Mohamed, A. Hashem, Removal of Methylene Blue Dye from Contaminated Wastewater using Lignocellulosic Biomasses: A Comparative Study Removal of Methylene Blue Dye from Contaminated Wastewater using Lignocellulosic Biomasses: A Comparative Study, 2024 May, https://doi.org/10.1016/j.wmb.2024.05.003.
- [6] S. Rodríguez-Couto, J.F. Osma, J.L. Toca-Herrera, Removal of synthetic dyes by an eco-friendly strategy, Eng. Life Sci. 9 (2) (2009) 116–123, https://doi.org/ 10.1002/elsc.200800088.

- [7] R. Ahmad, R. Kumar, Adsorption studies of hazardous malachite green onto treated ginger waste, J. Environ. Manag. 91 (4) (2010) 1032–1038, https://doi.org/ 10.1016/j.jenvman.2009.12.016.
- [8] K. Laachach, A. Alaoui, A. Azzi, Removal of methylene blue from aqueous solution using ghassoul, a low-cost adsorbent 8 (2) (2010) 153–163.
- [9] P. Sharma, H. Kaur, A Review on Applicability of Naturally Available Adsorbents for the Removal of Hazardous Dyes from Aqueous Waste, 2011, pp. 151–195, https://doi.org/10.1007/s10661-011-1914-0.
- [10] J. Fito, S. Abrham, K. Angassa, Adsorption of methylene blue from textile industrial wastewater onto activated carbon of *Parthenium hysterophorus*, Int. J. Environ. Res. 14 (5) (2020) 501–511, https://doi.org/10.1007/s41742-020-00273-2.
- [11] J. Fito, et al., Adsorption of methylene blue from textile industrial wastewater using activated carbon developed from Rumex abyssinicus plant, Sci. Rep. 13 (1) (2023) 1–17, https://doi.org/10.1038/s41598-023-32341-w.
- [12] S. Mohammad Momina, I. Suzylawati, Study of the adsorption/desorption of MB dye solution using bentonite adsorbent coating, J Water Process Eng 34 (January) (2020), https://doi.org/10.1016/j.jwpe.2020.101155.
- [13] N. Aishah Zarime, et al., Adsorption of methylene blue by bentonite supported nano zero valent iron (B-nZVI), Processes 11 (3) (2023) 1–14, https://doi.org/10.3390/nr11030788
- [14] C. Ponraj, G. Vinitha, J. Daniel, A review on the visible light active BiFeO3 nanostructures as suitable photocatalyst in the degradation of different textile dyes, Environ. Nanotechnol. Monit. Manag. 7 (2017) 110–120, https://doi.org/10.1016/j.enpm.2017.02.001.
- [15] Abdulrakib Abdulwahab Masad Al-Wahbi, Removal of methylene blue from aqueous solutions using Yemen bentonite, Diyala J. Eng. Sci. 4 (1) (2011) 30–53, https://doi.org/10.24237/djes.2011.04103.
- [16] S. Al-Asheh, F. Banat, L. Abu-Aitah, The removal of methylene blue dye from aqueous solutions using activated and non-activated bentonites, Adsorpt. Sci. Technol. 21 (5) (2003) 451–462, https://doi.org/10.1260/026361703769645780.
- [17] H.A. Hmeid, et al., Adsorption of a basic dye, methylene blue, in aqueous solution on bentonite, Moroccan J. Chem. 9 (3) (2021) 416–433.
- [18] A.J. Ibrahim, H.A.W. Dwesh, A.R.Y. Al-Sawad, Adsorption of methylene blue dye onto bentonite clay: characterization, adsorption isotherms, and thermodynamics study by using UV-vis technique, Anal. Methods Environ. Chem. J. 6 (3) (2023) 5–18, https://doi.org/10.24200/amecj.v6.i03.243.
- [19] A.H. Jawad, S.E.M. Saber, A.S. Abdulhameed, A.M. Farhan, Z.A. ALOthman, L. D. Wilson, Characterization and applicability of the natural Iraqi bentonite clay for toxic cationic dye removal: adsorption kinetic and isotherm study, J. King Saud Univ. Sci. 35 (4) (2023) 102630, https://doi.org/10.1016/j.jksus.2023.102630.
- [20] A.A. Jangher, S.M. Aghila, H.A. Jamhour, B.M. Mahara, Performance of Libyan bentonite as adsorbent for methylene blue dye: isotherms, kinetics and thermodynamic studies, Acad. J. Chem. 81 (2023) 1–11, https://doi.org/ 10.32861/aic.81.1.11.
- [21] H.N. Hamad, et al., Optimized bentonite clay adsorbents for methylene blue removal, Processes 12 (4) (2024), https://doi.org/10.3390/pr12040738.
- [22] H. Ouaddari, B. Abbou, I. Lebkiri, A. Habsaoui, M. Ouzzine, R. Fath Allah, Removal of methylene blue by adsorption onto natural and purified clays: kinetic and thermodynamic study, Chem. Phys. Impact 8 (December 2023) (2024) 100405, https://doi.org/10.1016/j.chphi.2023.100405.
- [23] B. Lou, et al., Solubility measurement and molecular simulation of unsolvated and solvated estrogen receptor agonist (R)-equol in binary solvents (alcohols + nheptane) from 273.15 K to 333.15 K, J. Mol. Liq. 376 (2023) 121460, https://doi. org/10.1016/j.molliq.2023.121460.
- [24] H.H. Shaarawy, H.S. Hussein, E.A. Kader, N.H. Hussien, S.I. Hawash, Adsorption performance of coated bentonite via graphene oxide, Bull. Natl. Res. Cent. 44 (1) (2020), https://doi.org/10.1186/s42269-020-00299-8.
- [25] H. Hirama, R. Otahara, S. Kano, M. Hayase, H. Mekaru, Characterization of nanoparticle adsorption on polydimethylsiloxane-based microchannels, Sensors 21 (6) (2021) 1–14, https://doi.org/10.3390/s21061978.
- [26] Q. Jia, D. Liu, Y. Cai, Y. Zhou, Z. Zhao, Y. Yang, AFM characterization of physical properties in coal adsorbed with different cations induced by electric pulse fracturing, Fuel 327 (July) (2022) 125247, https://doi.org/10.1016/j. fivel_2022_125247
- [27] H. Niwa, S. Ogawa, K. Nakanishi, G. Kutluk, T. Ohta, S. Yagi, Fabrication of rh nanoparticle and adsorption reaction with DMS studied by NEXAFS and XPS, J. Surf. Anal. 17 (3) (2011) 278–281, https://doi.org/10.1384/jsa.17.278.
- [28] A.S. Zdravković, N.J. Stanković, N.N. Ristić, G.M. Petković, Application of activated bentonite for the removal of direct and reactive dye from aqueous solutions, Chem. Ind. Chem. Eng. Q. 25 (4) (2019) 341–351, https://doi.org/ 10.2298/CICEQ171025012Z.
- [29] F.G. Alabarse, R.V. Conceição, N.M. Balzaretti, F. Schenato, A.M. Xavier, In-situ FTIR analyses of bentonite under high-pressure, Appl. Clay Sci. 51 (1–2) (2011) 202–208, https://doi.org/10.1016/j.clay.2010.11.017.
- [30] C.A. Buckner, et al., We are IntechOpen, the world 's leading publisher of Open Access books Built by scientists, for scientists TOP 1%, Intech 11 (tourism) (2016) 13 [Online]. Available, https://www.intechopen.com/books/advanced-biomet ric-technologies/liveness-detection-in-biometrics.
- [31] E.A. Abdelrahman, R.M. Hegazey, R.E. El-Azabawy, Efficient removal of methylene blue dye from aqueous media using Fe/Si, Cr/Si, Ni/Si, and Zn/Si amorphous novel adsorbents, J. Mater. Res. Technol. 8 (6) (2019) 5301–5313, https://doi.org/ 10.1016/j.jmrt.2019.08.051.
- [32] M. Said, W.T. Rizki, W. Purwaningrum, A. Rachmat, F. Ferlinahayati, P.L. Hariani, Modification bentonite using Fe(III) and its application as adsorbent for phenol, Mediterr. J. Chem. 9 (6) (2020) 422–431, https://doi.org/10.13171/ mjc9602001021024ms.

- [33] T. Taher, D. Rohendi, R. Mohadi, A. Lesbani, Thermal and acid activation (TAA) of bentonite as adsorbent for removal of methylene blue: a kinetics and thermodynamic study, Chiang Mai J. Sci. 45 (4) (2018) 1770–1781.
- [34] A. Bavi, M. Ghorbanpour, M.J.A. Alatabe, Adsorption, isotherms and kinetics characteristics of solid state Mg exchanged bentonite for removal of methylene blue, J. Water Environ. Nanotechnol. 8 (4) (2023) 396–405, https://doi.org/ 10.22000/INENT.2023.04.006
- [35] H. Zaitan, D. Bianchi, O. Achak, T. Chafik, A comparative study of the adsorption and desorption of o-xylene onto bentonite clay and alumina, J. Hazard. Mater. 153 (1–2) (2008) 852–859, https://doi.org/10.1016/j.jhazmat.2007.09.070.
- [36] P.B. Arthi G, et al., Novel graphene oxide/bentonite composite for uranium(VI) adsorption from aqueous solution, J. Radioanal. Nucl. Chem. 00 (3) (2020) 1349–1360, https://doi.org/10.1007/s10967-018-5992-0.
- [37] R. Wolski, A. Bazan-Wozniak, R. Pietrzak, Adsorption of methyl red and methylene blue on carbon bioadsorbents obtained from biogas plant waste materials, Molecules 28 (18) (2023), https://doi.org/10.3390/molecules28186712.
- [38] S. Al-Asheh, F. Banat, L. Abu-Aitah, Adsorption of phenol using different types of activated bentonites, Sep. Purif. Technol. 33 (1) (2003) 1–10, https://doi.org/ 10.1016/S1383-5866(02)00180-6.
- [39] J.R. Palembang-prabumulih, O. Ilir, Adsorption of phenol pollutants from aqueous solution using Ca-Bentonite / Chitosan composite (Adsorpsi Polutan Fenol dari Larutan Berair Menggunakan Komposit Ca-Bentonit / Kitosan) Poedji Loekitowati Hariani *, Fatma, Fahma Riyanti and Hesti Ratnasar 22 (2) (2015) 233–239.
- [40] F. Ademiluyi, S. Amadi, N. Amakama, Adsorption and treatment of organic contaminants using activated carbon from waste Nigerian bamboo, J. Appl. Sci. Environ. Manag. 13 (3) (2010), https://doi.org/10.4314/jasem.v13i3.55351.
- [41] E. Rápó, S. Tonk, Factors affecting synthetic dye adsorption; desorption studies: a review of results from the last five years (2017–2021), Molecules 26 (17) (2021), https://doi.org/10.3390/molecules26175419.
- [42] P. Senthil Kumar, C. Vincent, K. Kirthika, K. Sathish Kumar, Kinetics and equilibrium studies of Pb2+ ion removal from aqueous solutions by use of nanosilversol-coated activated carbon, Braz. J. Chem. Eng. 27 (2) (2010) 339–346, https://doi.org/10.1590/s0104-66322010000200012.
- [43] M. De La Luz-Asunción, V. Sánchez-Mendieta, A.L. Martínez-Hernández, V. M. Castaño, C. Velasco-Santos, Adsorption of phenol from aqueous solutions by carbon nanomaterials of one and two dimensions: kinetic and equilibrium studies, J. Nanomater. 2015 (2015), https://doi.org/10.1155/2015/405036.
- [44] H.N. Catherine, M.H. Ou, B. Manu, Y. Hsin Shih, Adsorption mechanism of emerging and conventional phenolic compounds on graphene oxide nanoflakes in water, Sci. Total Environ. 635 (2018) 629–638, https://doi.org/10.1016/j. scitotenv.2018.03.389.
- [45] A.A. Inyinbor, F.A. Adekola, G.A. Olatunji, Kinetics, isotherms and thermodynamic modeling of liquid phase adsorption of rhodamine B dye onto Raphia hookerie fruit epicarp, Water Resour. Ind. 15 (2016) 14–27, https://doi.org/10.1016/j. wri.2016.06.001.
- [46] J. Rojas, D. Suarez, A. Moreno, J. Silva-Agredo, R.A. Torres-Palma, Kinetics, isotherms and thermodynamic modeling of liquid phase adsorption of crystal violet dye onto shrimp-waste in its raw, pyrolyzed material and activated charcoals, Appl. Sci. 9 (24) (2019), https://doi.org/10.3390/app9245337.
 [47] W. Peng, H. Li, Y. Liu, S. Song, Adsorption of methylene blue on graphene oxide
- [47] W. Peng, H. Li, Y. Liu, S. Song, Adsorption of methylene blue on graphene oxide prepared from amorphous graphite: effects of pH and foreign ions, J. Mol. Liq. 221 (2016) 82–87, https://doi.org/10.1016/j.molliq.2016.05.074.
- [48] H. Asnaoui, Y. Dehmani, M. Khalis, E.K. Hachem, Adsorption of phenol from aqueous solutions by Na-bentonite: kinetic, equilibrium and thermodynamic studies, Int. J. Environ. Anal. Chem. 00 (00) (2020) 1–15, https://doi.org/ 10.1080/03067319.2020.1763328.
- [49] C. Wang, J. Li, L. Wang, X. Sun, J. Huang, Adsorption of dye from wastewater by zeolites synthesized from Fly ash: kinetic and equilibrium studies, Chin. J. Chem. Eng. 17 (3) (2009) 513–521, https://doi.org/10.1016/S1004-9541(08)60239-6.
- [50] H.W. Ayoob, A.M. Ridha, A.A. Jassim, N.K. Taieh, R.Z. Homod, H.I. Mohammed, Enhanced adsorption of phenol using graphene oxide-bentonite nanocomposites: synthesis, characterisation, and optimisation, J. Mol. Liq. 395 (November) (2023) 2024, https://doi.org/10.1016/j.molliq.2023.123833.
- [51] S.F.A. Shattar, N.A. Zakaria, K.Y. Foo, One step acid activation of bentonite derived adsorbent for the effective remediation of the new generation of industrial pesticides, Sci. Rep. 10 (1) (2020) 1–13, https://doi.org/10.1038/s41598-020-76733-w
- [52] M.A.L. Dutra, N.N. do Marques, M.S.M. de Souza Filho, R.C. de Balaban, Phenol removal from wastewater using eco-friendly hybrid hydrogels, J. Appl. Polym. Sci. 138 (30) (2021) 1–7, https://doi.org/10.1002/app.50725.
- [53] J.M. Li, X.G. Meng, C.W. Hu, J. Du, Adsorption of phenol, p-chlorophenol and p-nitrophenol onto functional chitosan, Bioresour. Technol. 100 (3) (2009) 1168–1173, https://doi.org/10.1016/j.biortech.2008.09.015.
- [54] D. A.O, Langmuir, Freundlich, Temkin and Dubinin-Radushkevich Isotherms Studies of Equilibrium Sorption of Zn 2+ Unto Phosphoric Acid Modified Rice Husk, IOSR J. Appl. Chem. 3 (1) (2012) 38–45, https://doi.org/10.9790/5736-0313845.
- [55] O. Idoko, M.O. Ajana, J.S. Gushit, A. Jock, Adsorption of heavy metals (Lead ion) from industrial waste water using acidified bentonite clay, Int. J. Eng. Appl. Sci. Technol. 04 (04) (2019) 394–401, https://doi.org/10.33564/ijeast.2019. vpdi/d 063
- [56] Z.L. Cheng, Y.X. Li, Z. Liu, Novel adsorption materials based on graphene oxide/ Beta zeolite composite materials and their adsorption performance for rhodamine B, J. Alloys Compd. 708 (2017) 255–263, https://doi.org/10.1016/j. jallcom.2017.03.004.

- [57] J. Wei, M.F. Aly Aboud, I. Shakir, Z. Tong, Y. Xu, Graphene oxide-supported Organo-montmorillonite composites for the removal of Pb(II), Cd(II), and As(V) Contaminants from Water, ACS Appl. Nano Mater. 3 (1) (2020) 806–813, https://doi.org/10.1021/acsanm.9b02311.
- [58] L. Tabana, S. Tichapondwa, F. Labuschagne, E. Chirwa, Adsorption of phenol fromwastewater using calcined magnesium-zinc-aluminium layered double hydroxide clay, Sustain 12 (10) (2020), https://doi.org/10.3390/su12104273.
- [59] M.O. Ansari, et al., Anion selective pTSA doped polyaniline@graphene oxide-multiwalled carbon nanotube composite for Cr(VI) and Congo red adsorption, J. Colloid Interface Sci. 496 (Vi) (2017) 407–415, https://doi.org/10.1016/j.jcis.2017.02.034.
- [60] K. Al-Essa, Activation of Jordanian bentonite by hydrochloric acid and its potential for olive mill wastewater enhanced treatment, J. Chemother. 2018 (2018), https://doi.org/10.1155/2018/8385692.
- [61] A. Mandal, N. Bar, S.K. Das, Phenol removal from wastewater using low-cost natural bioadsorbent neem (Azadirachta indica) leaves: adsorption study and MLR modeling, Sustain. Chem. Pharm. 17, no. September (2020) 100308, https://doi. org/10.1016/j.scp.2020.100308.
- [62] L. Chen, Y. Huang, L. Huang, B. Liu, G. Wang, S. Yu, Characterization of Co(II) removal from aqueous solution using bentonite/iron oxide magnetic composites, J. Radioanal. Nucl. Chem. 290 (3) (2011) 675–684, https://doi.org/10.1007/s10967-011-1337-y.
- [63] N.H. Yarkandi, Removal of lead (II) from waste water by adsorption, Int. J. Curr. Microbiol. App. Sci. 3 (4) (2014) 207–228.
- [64] H. Wang, H. Tang, Z. Liu, X. Zhang, Z. Hao, Z. Liu, Removal of cobalt(II) ion from aqueous solution by chitosan-montmorillonite, J. Environ. Sci. (China) 26 (9) (2014) 1879–1884, https://doi.org/10.1016/j.jes.2014.06.021.
- [65] L.B. Almalike, A.A. Al-Asadi, A.S. Abdullah, Adsorption of lead and cadmium ions onto soils: isotherm models, and thermodynamic studies, Gazi Univ. J. Sci. 33 (4) (2020) 702–717, https://doi.org/10.35378/gujs.650923.
- [66] G. Crini, E. Lichtfouse, Advantages and disadvantages of techniques used for wastewater treatment, Environ. Chem. Lett. 17 (1) (2019) 145–155, https://doi. org/10.1007/s10311-018-0785-9.

- [67] Y. Li, et al., Equilibrium, kinetic and thermodynamic studies on the adsorption of phenol onto graphene, Mater. Res. Bull. 47 (8) (2012) 1898–1904, https://doi.org/ 10.1016/j.materresbull.2012.04.021.
- [68] A.M. Aljeboree, A.N. Alshirifi, A.F. Alkaim, Kinetics and equilibrium study for the adsorption of textile dyes on coconut shell activated carbon, Arab. J. Chem. 10 (2017) S3381–S3393, https://doi.org/10.1016/j.arabjc.2014.01.020.
- [69] V.J. Inglezakis, A.A. Zorpas, Heat of adsorption, adsorption energy and activation energy in adsorption and ion exchange systems, Desalin. Water Treat. 39 (1–3) (2012) 149–157, https://doi.org/10.1080/19443994.2012.669169.
- [70] C.R. Girish, Determination of thermodynamic parameters in adsorption studies: a review, Chem. Pap. (0123456789) (2025), https://doi.org/10.1007/s11696-025-04218-y
- [71] M.A. Al-Ghouti, D.A. Da'ana, Guidelines for the use and interpretation of adsorption isotherm models: a review, J. Hazard. Mater. 393 (January) (2020) 122383, https://doi.org/10.1016/j.jhazmat.2020.122383.
- [72] M. Vigdorowitsch, A. Pchelintsev, L. Tsygankova, E. Tanygina, Freundlich isotherm: an adsorption model complete framework, Appl. Sci. 11 (17) (2021) 1–7, https://doi.org/10.3390/app11178078.
- [73] P.B.A. Abdul Ghani, R. Rusmin, I.S. Izman, Desorption studies for methylene blue dye removal by kaolinite, Sci. Res. J. 18 (2) (2021) 215–227, https://doi.org/ 10.24191/srj.v18i2.14127.
- [74] S. Mohammad Momina, I. Suzylawati, Study of the adsorption/desorption of MB dye solution using bentonite adsorbent coating, J Water Process Eng 34 (July) (2019) 2020, https://doi.org/10.1016/j.jwpe.2020.101155.
- [75] U.F. Alkaram, A.A. Mukhlis, A.H. Al-dujaili, The removal of phenol from aqueous solutions by adsorption using surfactant-modified bentonite and kaolinite 169 (2009) 324–332, https://doi.org/10.1016/j.jhazmat.2009.03.153.
- [76] C. Suryanarayana, Mechanical alloying and milling, Mech. Alloy. Milling (May) (2004) 1–472, https://doi.org/10.4150/kpmi.2006.13.5.371.
- [77] T. Tsuzuki, P.G. McCormick, Mechanochemical synthesis of nanoparticles, J. Mater. Sci. 39 (16) (2004) 5143–5146.